Journal of Materials Chemistry C

Highly Fluorescent Nitrogen-Doped Carbon Dots with Large Stokes Shift

Journal:	*Journal of Materials Chemistry C*
Manuscript ID	TC-ART-06-2023-002209.R1
Article Type:	Paper
Date Submitted by the Author:	26-Jul-2023
Complete List of Authors:	Zhang, Xueqiao; Oregon State University Liu, Ye; Oregon State University, Electrical Engineering Kuan, Chieh-Hsi; Oregon State University Tang, Longteng; Oregon State University, Department of Chemistry Krueger, Taylor; Oregon State University Yeasmin, Sanjida; Oregon State University Ullah, Ahasan; Oregon State University Fang, Chong; Oregon State University, Department of Chemistry; Oregon State University, Department of Physics Cheng, Li-Jing; Oregon State University, Electrical Engineering and Computer Science; Oregon State University

ARTICLE

Highly Fluorescent Nitrogen-Doped Carbon Dots with Large Stokes Shift

Received 00th January 20xx,
Accepted 00th January 20xx

DOI: 10.1039/x0xx00000x

Xueqiao Zhang,[a†] Ye Liu,[a†] Chieh-Hsi Kuan,[b] Longteng Tang,[b] Taylor D. Krueger,[b] Sanjida Yeasmin,[a] Ahasan Ullah,[a] Chong Fang,[b] and Li-Jing Cheng*[a]

Carbon dots (CDs) are eco-friendly luminescent materials with the potential to replace traditional phosphors and heavy metal-based quantum dots in color-conversion light-emitting devices (LEDs). The color-conversion LEDs require the luminescent material with sufficiently large Stokes shift to efficiently absorb blue or UV excitation and emit longer wavelengths, the photoluminescence mechanism of which is not widely studied for red emissive CDs. This work demonstrates a new type of red carbon dots (R-CDs) with a large Stokes shift synthesized by a solvothermal reaction of 3,4-dihydroxy-L-phenylalanine and urea in dimethylformamide. The R-CDs were measured to be 5.5 nm-sized multilayer nitrogen-doped graphene nanodots with an emission peak of 623 nm. We exfoliated the R-CDs to produce monolayer graphene nanodots through an alkaline post-treatment, yielding green carbon dots (G-CDs) with a 511 nm emission peak. Remarkably, the R-CDs and G-CDs exhibit large Stokes shifts of 216 nm (1.06 eV) and 140 nm (0.92 eV), along with high quantum yields of 45.2% and 24.1%, respectively. The large Stokes shift can be ascribed to the emission through the surface states contributed by the carbonyl and nitrogen-based surface functional groups, which have lower energy than the excitation through the edge and core states of the CDs. The leading role of surface-state-derived emission was confirmed by pH-dependent emission wavelength of the R-CDs and femtosecond transient absorption measurements. Furthermore, we demonstrated the use of printable CD inks to create microscale multicolor patterns and color-conversion LEDs, indicating the substantial potential for display applications.

Introduction

Carbon dots (CDs) are cost-effective and environmentally friendly carbon-based fluorescent nanomaterials that can be produced to exhibit high quantum yield, high photostability, and tunable fluorescence emission.[1–3] They have a strong potential to replace conventional phosphors and quantum dots (QDs) in color conversion light-emitting diodes (LEDs) and micro-LED displays.[4–8] Full-color micro-LEDs can be realized using photoluminescence (PL), which utilizes color down-conversion media, such as QDs, to convert blue or ultraviolet (UV) light into red and green emission.[9,10] High-efficiency color-conversion LEDs require luminescent materials with high PL quantum yield (QY) and large Stokes shift to efficiently absorb blue or UV excitation and emit longer wavelength light. In addition to their applications in LEDs and displays, CDs with a large Stokes shift, high quantum yield, and broad absorption spectrum emerge as promising candidates for luminescent solar concentrators.[11,12]

Recent advancements in CDs have primarily focused on expanding the emission range to include near-infrared,[13] narrowing emission bandwidth,[14] simplifying synthesis procedures, etc.[15] However, research dedicated explicitly to large Stokes shift CDs remains limited. One of the strategies to enlarge the Stokes shift involves introducing moieties that promote charge transfer through vibrational relaxation, thereby increasing the difference between the excitation and emission energies. Wen et al. synthesized green emissive carbon dots with a notable Stokes shift of 230 nm, ascribed to the electron transfer through vibrational relaxation to the surface states for emission.[16] Note that a more accurate way to represent the Stokes shift is in energy units like eV or cm^{-1}. However, for this summary, we have provided the reported values described in the literature. Xiao et al. developed yellow emissive carbon dots doped with Cl and N, exhibiting a large Stokes shift of 177 nm.[17] Hu et al. utilized the precursor with a symmetry-breaking electronic structure for red CDs synthesis to increase the Stokes shift from 75 nm to 161 nm.[18] Ali et al. demonstrated red CDs with a Stokes shift of 100 nm by modifying the surface states.[19] Despite these findings, limited comprehensive research is available on red emissive CDs with significant Stokes shifts.

Here we demonstrate a new type of red emissive CDs (R-CDs) and green emissive CDs (G-CDs) with large Stokes shifts achieved by introducing nitrogen (N)-dopants and oxygen (O)-

[a] School of Electrical Engineering and Computer Science, Oregon State University, Corvallis, Oregon 97331, USA. Email: chengli@oregonstate.edu
[b] Department of Chemistry, Oregon State University, Corvallis, Oregon 97331, USA
† These authors contribute equally.
Electronic Supplementary Information (ESI) available: [details of any supplementary information available should be included here]. See DOI: 10.1039/x0xx00000x

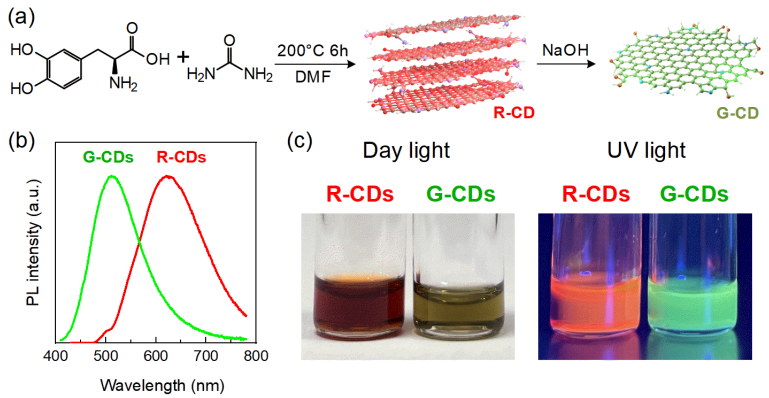

Figure 1. (a) Synthesis route of the R-CDs and G-CDs by a solvothermal method using L-dopa and urea precursors. (b) Normalized PL spectra of R-CDs and G-CDs excited at 407 nm and 371 nm, respectively. (c) Photographs of the R-CDs and G-CDs in chloroform under daylight (left) and 395 nm UV light (right).

functional groups to enable excitation through the edge states of the CDs[20,21] and emission through the surface states. The N-doped CDs were synthesized by a solvothermal reaction of 3,4-dihydroxy-L-phenylalanine (L-dopa) and urea in dimethylformamide (DMF). The reaction resulted in R-CDs composed of multilayer N-doped graphene nanodots with a 623 nm emission peak. The R-CDs can be further exfoliated to produce single-layer graphene nanodots, yielding green emissive CDs (G-CDs) with an emission peak of 511 nm. The R-CDs and G-CDs both display large Stokes shifts of 216 and 140 nm, respectively, along with high QYs of 45.2% and 24.1%. The large Stokes shift enables R-CDs and G-CDs to efficiently absorb UV and blue excitation light ranging from 390 to 450 nm. These wavelengths correspond to the excitations used in color-conversion micro-LEDs. Compared to previously reported CDs with large Stokes shift,[14,16–19,22–30] the CDs presented here achieve the highest value. Material analysis suggests that carbonyl and nitrogen-containing functional groups, including amide and C=N bonds, on the R-CD surfaces contribute to the emission derived from surface states. The surface states have lower energy than the excitation through the edge states at the boundary between the sp^2- and sp^3-hybridized carbon of the CDs. The pH-dependent emission of the R-CDs confirms the significant influence of surface functional groups on the emission wavelength. Surface states facilitate radiative recombination following vibrational relaxation, resulting in low-energy emission and a substantial Stokes shift. To demonstrate their versatility, the CDs were utilized to formulate nanocomposite inks, enabling the creation of printable microscale luminescent patterns and PL-based LEDs.

Results and discussion

Preparation of R-CDs and G-CDs

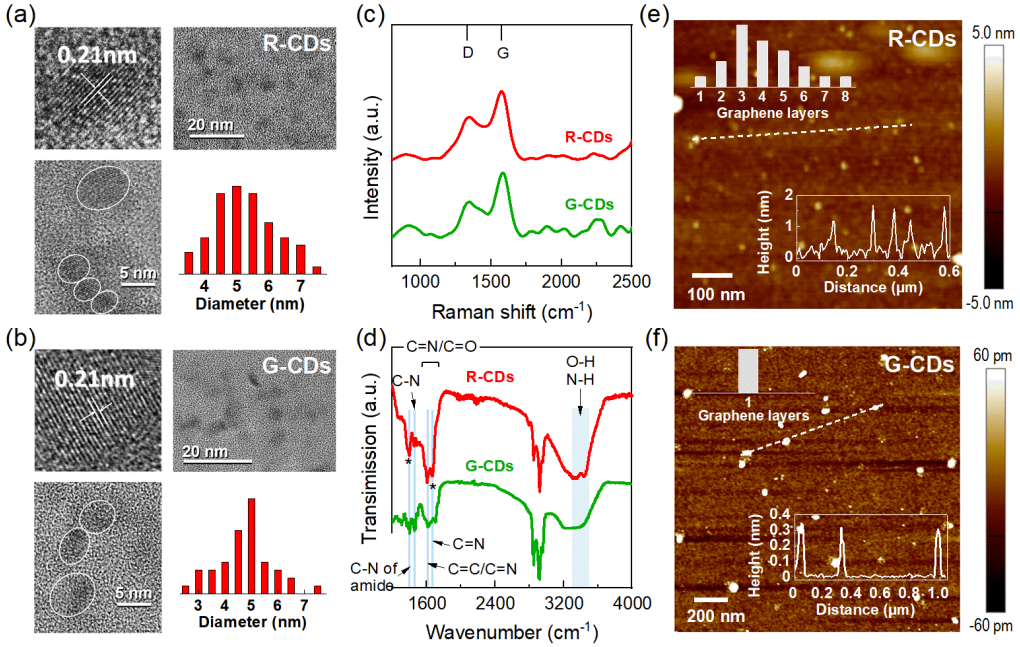

Figure 2. TEM images of (a) R-CDs and (b) G-CDs with high-resolution TEM images and particle size distributions (red histograms). (c) Raman and (d) FTIR spectra of R-CDs (red) and G-CDs (green lines). Key vibrational marker bands are indicated by semi-transparent blue shades. AFM images of (e) R-CDs and (f) G-CDs. The insets show the representative height profiles measured along the dash lines (bottom right) and height distribution profiles of more than 30 CDs (top left).

The R-CDs were prepared by a solvothermal method detailed in the experimental section. The reaction started with condensing N-containing materials L-dopa and urea, which were then carbonized to form the CDs, as illustrated in **Figure 1a**. The R-CDs precipitates were extracted after rinsing with dichloromethane (DCM) and DI water. The R-CDs were further exfoliated to generate G-CDs with a QY of 24.1% through a post-treatment in sodium hydroxide.

We synthesized R-CDs with various urea to L-dopa weight ratios (1:0.2, 1:0.4, 1:0.6, 1:1, 1:2, 1:3) to determine the optimal precursor ratio for achieving the best PL performance. **Figure S1** and **Table S1** show that different precursor ratios yielded similar absorption, excitation, and emission characteristics but distinct QYs. Among the ratios tested, the 1:1 urea to L-dopa ratio produced the highest QY and was selected as the optimal condition for the subsequent experiment. The PL spectra in **Figure 1b** demonstrate that the R-CDs emit at 623 nm under 407 nm excitation, while the G-CDs emit at 511 nm under 371 nm excitation. **Figure 1c** presents photographs of the CDs solution in chloroform captured under daylight and UV irradiation.

Material Characterizations of CDs

The structure and composition of CDs were confirmed through transmission electron microscopy (TEM). The TEM images in **Figure 2a** and **2b** reveal that the CDs are carbon nanodots with average diameters of 5.5 nm for R-CDs and 5.0 nm for G-CDs. The reduced particle size in G-CDs may result from the exfoliation of R-CDs during the post-treatment process. High-resolution TEM analysis unveiled a crystal structure with a lattice spacing of approximately 0.21 nm in both R-CDs and G-CDs. This spacing corresponds to the (100) facet of graphite, indicating the presence of graphite structures in both types of CDs.[13,31]

The Raman spectra in **Figure 2c** indicate that both R-CDs and G-CDs possess a graphene structure, evidenced by the presence of two Raman peaks: the G band at 1584 cm^{-1}, which corresponds to the planar sp^2-bonded carbon characteristic of graphene, and the D band at 1348 cm^{-1}, which signifies disordered structure within the sp^2-hybridized graphene carbon system.[32,33] The G/D ratios calculated from the band areas are about 2.05 for R-CDs and 2.1 for G-CDs, indicating a high degree of graphitization, which distinguishes them from other reported CDs.[29,34]

The Fourier transform infrared (FTIR) spectra in **Figure 2d** demonstrate that R-CDs and G-CDs share similar functional groups and compositions. Both exhibit broad peaks ranging from 3000 to 3500 cm^{-1}, attributed to O–H and N–H stretching vibrations from amine groups. Multiple peaks between 1550 and 1750 cm^{-1} are evident for both CDs, corresponding to C=N stretching vibration at lower frequencies and C=O stretching vibrations at higher frequencies. We also observe a peak at 1630 cm^{-1} indicating vibrations of aromatic C=C bonds and C=N bonds in the basal plane,[35] along with C–N stretching vibrations at 1455 cm^{-1}.[36,37] In addition, two distinct peaks at 2851 and 2921 cm^{-1} correspond to CH_2 groups.[13,38] However, there are two noticeable differences between the R-CDs and the G-CDs. First, R-CDs exhibit stronger peaks associated with the vibrations of C–N (1392 cm^{-1}) groups from amides and a more noticeable N–H vibration from amines in the range of 3300–3500 cm^{-1}. The presence of these amide-based functional groups in R-CDs is linked to the notable emission redshift, which will be discussed later. Second, the stronger high-frequency band between 1550 and 1750 cm^{-1} and the 1656 cm^{-1} peak in

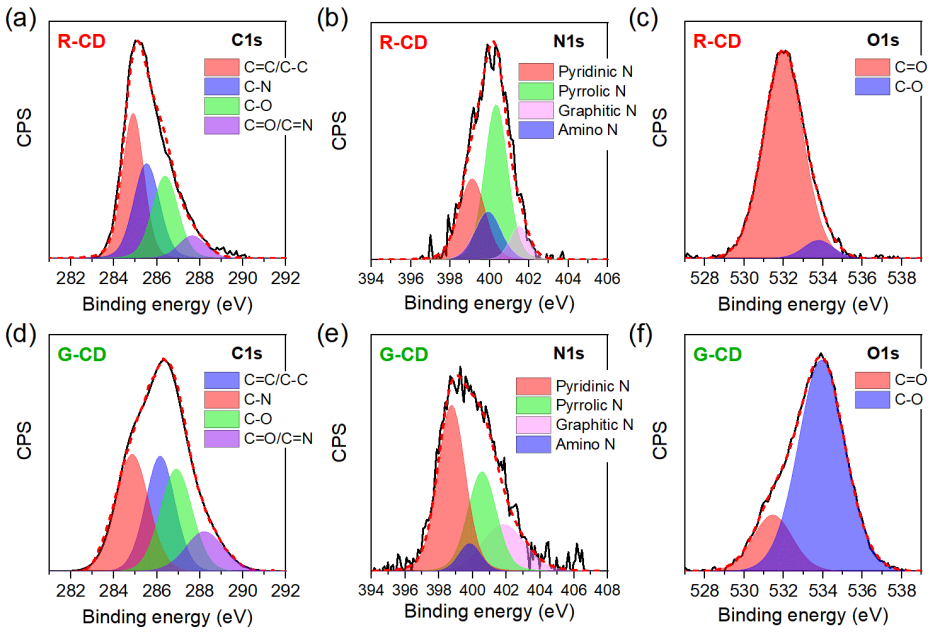

Figure 3.High-resolution XPS C1s, N1s, and O1s spectra of (a-c) R-CDs and (d-f) G-CDs. The individual components from the best gaussian fits are shown as semi-transparent color-coded shades with the overall XPS profile shown as thick red dashed line in each panel, overlaid with the spectral data in solid black line.

R-CDs imply a higher abundance of C=O surface groups, along with a strong C=N vibration related to mid-gap energy levels that contributes to the emission redshift of R-CDs.[39,40,41]

In **Figure 2e** and **2f**, the topographic images obtained through atomic force microscopy (AFM) analysis revealed that the R-CDs and G-CDs have average thicknesses around 1.35 and 0.34 nm, respectively. The result implies that R-CDs are 4-layer graphene nanoparticles while the G-CDs are monolayer graphene nanoparticles.[42] Note that the average thicknesses were calculated from more than 30 CD particles. **Figure S2** presents three additional height profiles measured on the R-CDs and G-CDs coated samples. The monolayer graphene structure of G-CDs was achieved through the exfoliation of R-CDs in sodium hydroxide (NaOH), as depicted in **Figure 1a**. The treatment involved the interaction of NaOH into the multilayer graphene structure, which weakened the van der Waals interplanar binding force between the graphene layers, thus separating the graphene layers with high exfoliation efficiency.[43]

The X-ray photoelectron spectroscopy (XPS) full spectra, as summarized in **Figure S3** and **Table S2**, show that both R-CDs and G-CDs primarily comprise carbon, oxygen, and nitrogen with similar elementary percentages. In the high-resolution XPS spectra of R-CDs in **Figure 3a-c**, the C1s band can be deconvoluted into four binding energy peaks corresponding to C=C/C–C (284.8 eV), C–N (285.4 eV), C–O (286.3 eV), and C=N/C=O (287.5 eV). The N1s band shows four peaks for pyridinic N (398.7 eV), amino N (399.8 eV), pyrrolic N (400.2 eV), and graphitic N (401.4 eV).[44,45] The O1s spectrum exhibits two peaks at 532.0 and 533.7 eV, attributed to C=O and C–O, respectively.[14,46] The high-resolution N spectrum indicates that R-CDs contain a higher proportion of pyrrolic N (**Figure 3b**), while G-CDs exhibit a larger amount of pyridinic N (**Figure 3e**). It has been reported that pyrrolic N dopants can decrease the bandgap of CDs,[47] in accord with the measured bandgaps (**Figure S4**) and the notable redshift observed in the absorption peak of R-CDs (**Figure S4a**) compared to G-CDs (**Figure S4b**). The high-resolution O1s spectrum analysis suggests that R-CDs contain a much higher proportion of C=O than C–O groups (**Figure 3c**), consistent with the FTIR results shown in **Figure 2d**. On the other hand, G-CDs have a more significant number of C–O groups (**Figure 3f**). The different oxygen functional groups between R-CDs and G-CDs can be attributed to the NaOH treatment, which converted the surface carbonyl groups to hydroxyl groups in G-CDs.[48]

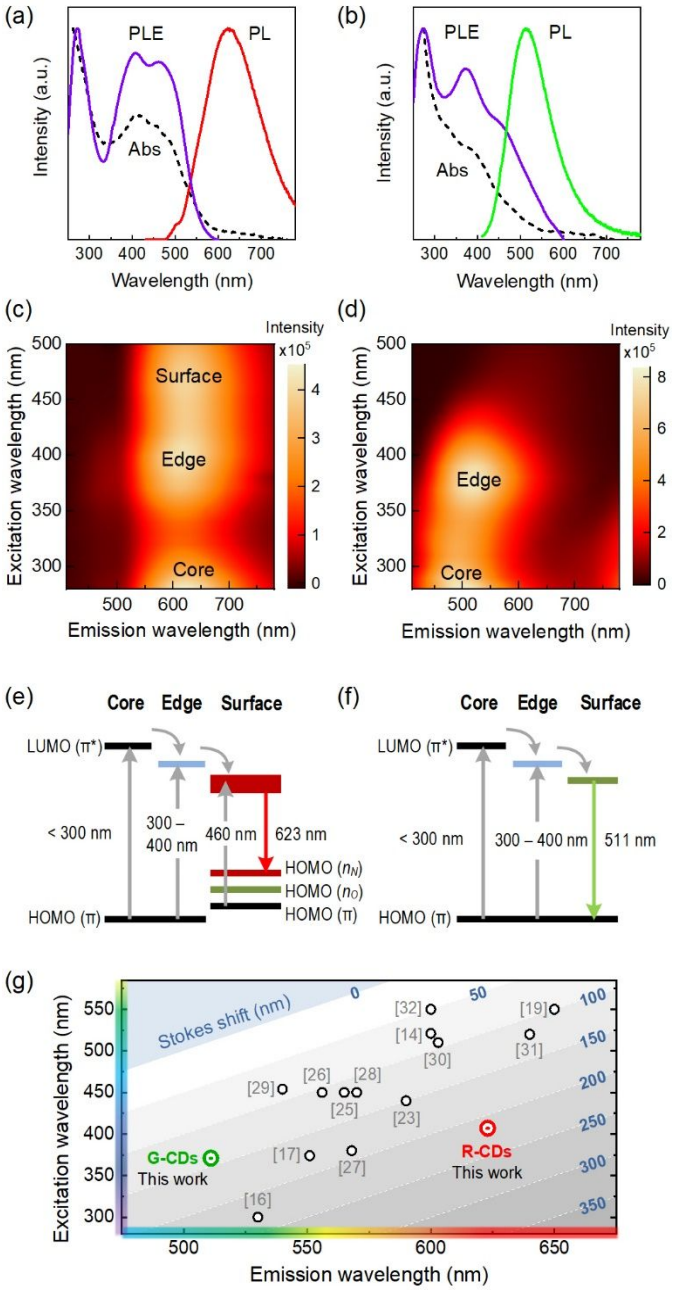

Figure 4. Absorption, PLE, and PL spectra of (a) R-CDs and (b) G-CDs. 2D-contour plots of PLE vs. PL spectra for (c) R-CDs and (d) G-CDs. Jablonski diagrams illustrate the excitation and emission processes of (e) R-CDs and (f) G-CDs. (g) Comparison of Stokes shift vs. emission/excitation wavelength between this work and previous reports (reference numbers denoted) of CDs with large Stokes shifts.

Photoluminescence Properties of CDs

Steady-state electronic absorption spectra show that R-CDs (**Figure 4a**) and G-CDs exhibit absorption in the UV and visible ranges but with distinct spectral features (**Figure 4a-b**). The strong absorption peak at about 270 nm corresponds to the π→π* transitions from the aromatic C=C bonds in the graphitic core of CDs.[49–51] Both CDs display a prominent absorption band between 300 and 400 nm, associated with the n→π* transitions through the non-bonding orbitals at the edge of the sp^2-hybridized core. These edge states originated from the boundary between the sp^2- and sp^3-hybridized carbon, where the surface functional groups connect to the sp^2-carbon lattice.[20,21]

R-CDs exhibit strong absorption at around 460 nm, ascribed to the low-energy transitions through the abundant C=O and C=N functional groups on the CD surface.[49,52,53] The C=O and C=N surface functional groups have been reported to decrease the

energy gap of CDs.[40,54] The 460 nm absorption band is significantly reduced in G-CDs, appearing as a small shoulder, due to the reduced amount of C=O groups, as observed in the XPS analysis (**Figure 3f**). The optical bandgaps extracted from Tauc plots (**Figure S4**) are 2.31 eV for R-CDs and 2.70 eV for G-CDs. The smaller optical bandgap in R-CDs explains the absorption peak redshift. Notably, the absorption profiles of both R-CDs and G-CDs align with their corresponding photoluminescence excitation (PLE) spectra, with the optimal excitation peak matching the absorption maximum. This observation suggests that the absorption-related structures are responsible for the excitation process.

The PLE vs. PL plots in **Figures 4c** and **4d** show that the emission wavelengths of R-CDs and G-CDs are predominantly unaffected by the excitation wavelength. The excitation-independent emission is likely attributed to the surface state-derived emission.[13] The emission maxima occur at 623 nm for R-CDs and 511 nm for G-CDs. The QYs of R-CDs and G-CDs were measured to be 45.2 and 24.1% under excitation wavelengths of 407 nm and 371 nm, respectively. Remarkably, both R-CDs and G-CDs exhibit large Stokes shifts of 216 nm (1.06 eV) and 140 nm (0.92 eV), respectively. In comparison to previous studies on CDs with large Stokes shifts,[14,16–19,22–30,55] the R-CDs reported here demonstrate the highest Stokes shift among the red emissive CDs (**Figure 4g** and **Table S3**).

Consistent with the absorption characteristics, both CDs reveal two strong PLE peaks originating from core-state transitions in the deep-UV range at ~270 nm and the edge-state transitions between 300 and 400 nm. Additionally, R-CDs exhibit another lower-energy surface state-derived excitation at 460 nm. The Jablonski diagrams in **Figures 4e** and **4f** illustrate the PL mechanism for R-CDs and G-CDs. Under UV excitation (< 300 nm wavelength), electrons are excited to the π* states in the carbogenic core.[13,16] Subsequently, the excited electrons undergo vibrational relaxation to the LUMO of the edge states and then to the LUMO of the surface states contributed by nitrogen[40,44,47,56] and oxygen functional groups, such as carbonyl and hydroxyl groups.[40,57] Finally, emission occurs when the electrons transit to the HOMO of the surface states through radiative recombination. Compared to G-CDs, R-CDs exhibit a higher abundance of carbonyl and amide groups at the CD surface. The amide groups result in a higher energy level in the HOMO (π) at the surface states, leading to a long-wavelength PLE peak at 460 nm.[41,49,54,58] Furthermore, the abundant C=N and C=O surface functional groups in R-CDs introduce additional orbital levels represented by the HOMO (n_N) and HOMO (n_O) in **Figure 4e**, which further decrease the LUMO-HOMO gap of the surface states.[40,41] The reduced energy gap results in a longer emission wavelength of 623 nm, in contrast to the 511 nm emission observed for G-CDs (**Figure 4f**). With the excitation mainly governed by core and edge states, while the emission is predominantly controlled by surface states with a reduced energy gap, the CDs exhibit significant Stokes shifts.

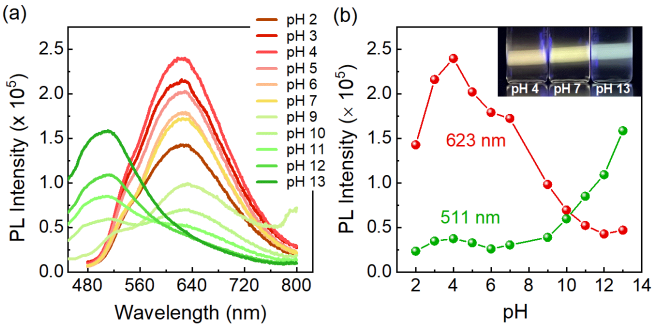

Figure 5. (a) PL spectra of R-CDs with pH varying from 2 to 13. (b) PL intensities at 623 (red) and 511 (green) nm of R-CDs at various pH levels. The inset displays a photo of the R-CD solutions at pH 4, pH 7 and pH 13 upon exposure to a 405 nm laser beam.

To confirm the impact of surface states on emission wavelength, we examined the PL properties of R-CDs under various pH conditions. The pH of the R-CDs solution in chloroform was adjusted using acetic acid and triethylenetetramine (TETA) while keeping the total volume constant at 2 mL. As shown in **Figure 5**, the emission peak of R-CDs remained consistent at around 623 nm under 407 nm excitation in neutral and acidic conditions. However, we observed an intriguing trend in the emission peak behavior with varying pH levels. Specifically, the 623 nm emission peak increased from pH 2 to 4 and gradually decreased from pH 4 to 10 (**Figure 5b**). As the solution shifted toward alkaline conditions, the 623 nm peak vanished, and a new and stronger PL peak at 511 nm emerged as the pH level increased from 9 to 13 (**Figure 5**). The pH-dependent emission can be attributed to the (de)protonation and tautomerism between the amide (–NH–C=O) and imidate (–N=C–OH) at the CD surface. The change in pH from acidic to alkaline conditions resulted in the conversion of amide groups to imidate groups, which, in turn, altered the surface states and influenced the emission wavelength.[13,59] The conversion of carbonyl to hydroxyl groups in amides, as evidenced by the changes observed in the O1s XPS spectra in **Figures 3c** and **3f**, results in diminished 623 nm emission and promoted 511 nm emission. These findings further support the connection between surface functional groups and the observed emission wavelengths in R-CDs and G-CDs.

Femtosecond transient absorption spectroscopy (fs-TA) was employed to gain deeper insights into the engineered CDs, demonstrating a large Stokes shift upon 400 nm excitation. The time-stacked fs-TA spectra of G-CDs and R-CDs after 400 nm excitation are provided in **Figure S5**. The fs-TA spectra and probe-dependent analysis are presented in **Figures 6a** and **6c** for G-CDs and **Figures 6b** and **6d** for R-CDs. The 2D-contour plot of G-CDs (**Figure 6a**) displays a broad exited-state absorption (ESA) band spanning from ~400 to 700 nm. The probe-dependent analysis was conducted to retrieve the weight and lifetime of each underlying component. Interestingly, the TA signal obtained from two probe regions of 473–478 nm (blue trace in **Figure 6c**) and 601–606 nm (red trace in **Figure 6c**) exhibits distinct dynamics, which can be assigned to the surface

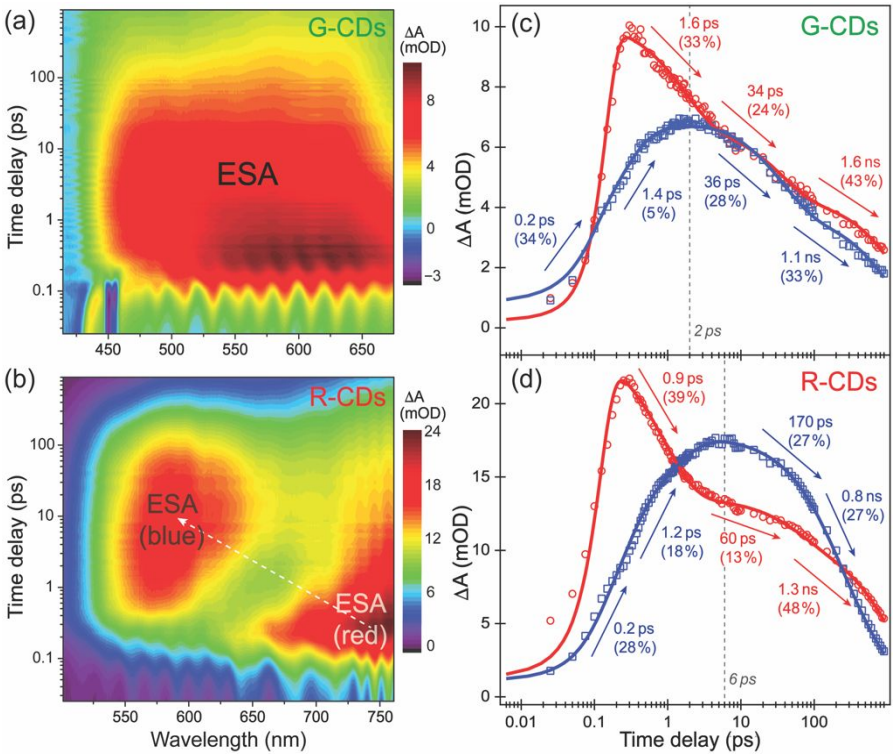

Figure 6. 2D-contour plots of fs-TA spectra of (a) G-CDs and (b) R-CDs after 400 nm excitation. The excited-state absorption (ESA) bands are pronounced, with the clear spectral evolution between a red ESA and blue ESA highlighted by a dashed white arrow in panel (b). Probe-dependent dynamics with the least-squares fits of fs-TA spectra for (c) G-CDs and (d) R-CDs. Experimental data from specific probe regions for G-CDs (blue squares: 473–478 nm, red circles: 601–606 nm) and R-CDs (blue squares: 584–588 nm, red circles: 733–739 nm) are overlaid with the best fits (color-coded solid curves). The time constants indicating individual temporal components and their associated amplitude weights are labeled near the arrows.

and edge states, respectively. Such a "crossing" pattern between two dynamic traces is manifested by the initial decay component of the red trace (1.6 ps, edge state) and one of the rising components of the blue trace (1.4 ps, surface state), indicative of a shared electronic transition process. However, after this initial crossover event, both ESA bands display a similar biphasic decay, implying that the environments of surface and edge states resemble each other after the presumably ultrafast charge-transfer (CT) event on the sub-ps to few ps timescales. This dynamic picture rationalizes the smaller Stokes shift of G-CDs, highlighted by the small magnitude (5% weight) of the 1.4 ps rise component for the surface state and the similar decay dynamics of both edge and surface states after ~2 ps (see vertical dashed line in **Figure 6c**).

In contrast, R-CDs exhibit two prominent ESA bands associated with the edge and surface states in the red and blue spectral regions, respectively. The crossover behavior is evident in the 2D-contour plot (**Figure 6b**). The blue ESA peak also displays a notable redshift, indicating excited-state relaxation events that reduce the upward transition energy gap (e.g., $S_1 \rightarrow S_2$). Similar to G-CDs, the probe-dependent fits for regions of 584–588 nm and 733–739 nm reveal discernible differences between the blue and red ESA bands. However, the edge-to-surface state crossover time constants shorten to ~0.9–1.2 ps (**Figure 6d**). Moreover, the rise component is more pronounced (18% weight) and reaches its peak value later (~6 ps) in R-CDs than in G-CDs (~2 ps). This suggests a more complete CT process in R-CDs, leading to a larger Stokes shift. The enhanced dynamics between the post-CT edge and surface states support this conclusion, affirming the significant Stokes shift observed in R-CDs. This is further supported by the distinct dynamics observed between the post-CT edge and surface states.

This CT event is corroborated by previous works using different techniques. Nguyen et al. detected energy flow (0.44 ps) in CDs via ultrafast nanometric imaging.[60] Wen et al. employed time-resolved photoluminescence to study excited-state dynamics of CDs and obtained the CT lifetime of 0.4 ps for ultrafast trapping from the sp^2-nano domains to the surface states.[61] Others conducted fs-TA to analyze the excited-state behaviors of CDs, and proposed the key role of the surface state with oxygen-containing functional groups in trapping the photoexcited electrons within 1 ps to emit strong fluorescence.[62]

Printable CD Inks and Applications

The large Stokes shift of the CDs enables efficient excitation using blue or UV light in color-conversion LEDs, ensuring minimal interference between the excitation wavelength and emission light. To prepare printable CD inks, we mixed the CDs with polyvinylpyrrolidone (PVP) polymer binders in DMF. The PVP binder provided the desired ink viscosity for printing and created a polymeric framework that facilitates the homogenous distribution of CDs, preventing fluorescence quenching. We

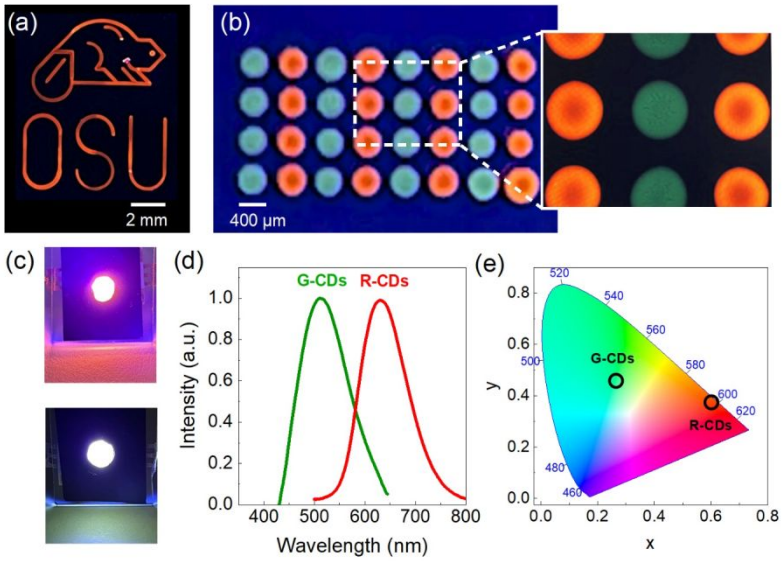

Figure 7. Microscopic images of the (a) printed fluorescent patterns and (b) dot array generated using the R-CD and G-CD inks. (c) Photographs of red and green down-conversion LEDs using UV LED excitation on the printed R-CD and G-CD layers. (f) Normalized PL spectra of R-CD and G-CD LEDs excited by 400 nm backlight LEDs. (g) Emission color coordinates of the two LEDs displayed on a CIE chromaticity diagram.

utilized a microplotter to dispense pico- and nanoliter-sized droplets of the CD inks to generate microscale fluorescent patterns on a glass substrate. The dispense speed and duration were optimized to control the printing resolution, resulting in the pre-designed patterns and microscale dot array, as shown in **Figures 7a** and **7b**. By depositing the CD inks on a UV LED backlight substrate, we developed color conversion layers for PL-based LEDs, as shown in **Figure 7c**. The CD layers effectively down-converted the 400 nm UV backlight to red and green emissions, which were confirmed by the PL spectra and CIE chromaticity diagrams of R-CDs and G-CDs LEDs, presented in **Figures 7d** and **7e**, respectively.

Experimental

Materials

The precursors, 3,4-dihydroxy-L-phenylalanine (L-dopa) and urea were purchased from Carbosynth and Alfa Aesar, respectively. Polyvinylpyrrolidone (PVP, Mn = 40000) was purchased from Alfa Aesar. Solvents including N,N-dimethylformamide (DMF), dichloromethane (DCM), chloroform, toluene, isopropanol, 1-propanol, acetone, ethanol, formamide, ethyl acetate, acetonitrile, dimethyl sulfoxide (DMSO), acetic acid, triethylenetetramine (TETA), were of analytical reagent grade and purchased from Sigma-Aldrich. All chemicals were used as received without further purification.

Preparation of CDs

The CDs were synthesized using a solvothermal method, starting with dissolving L-dopa (50 mg) and urea (50 mg) in DMF (4 mL) in a 4 mL glass vial. The glass vial was capped by a Teflon disk and enclosed in a Teflon-lined autoclave reactor for reaction at 200 °C for 6 h. The Teflon disk had a proper thickness to fill the gap between the glass vial and the lid of the Teflon chamber. The appropriate capping of the glass vial was critical for achieving a high yield in the reaction. After the reaction, the product was washed with dichloromethane (DCM) (3 mL) and DI water (7 mL). Centrifugation at 8000 rpm for 8 min facilitated the collection of the precipitate formed at the interface between the DCM and DI water layers. The obtained precipitate, named R-CDs, was then dried overnight at 60 °C to yield red fluorescent CDs. To obtain green CDs (G-CDs), the previously collected precipitate was dispersed in sodium hydroxide (2 mL, 5 mM) for 2 min. The resulting solution underwent the same protocol to collect the treated precipitate, which was subsequently dried at 60 °C overnight.

Preparation of Printable CD Inks

The polymeric binder for the CD inks was prepared by dispersing PVP (0.2 g) in DMF (1 ml) followed by 10 min sonication for a full dissolution. Then, the CDs (0.3 mg) were added to the PVP solution. The mixture was completely dispersed under sonication, forming the CD ink. The CD ink was applied to create pre-designed microscale patterns using a SonoPlot material printer and produce the color-conversion layers for the PL-based LEDs.

Characterization and Instruments

Absorption spectra were recorded using a Thermo Scientific NanoDrop 2000c spectrophotometer. PL and PLE spectra were measured using a spectrofluorometer (Horiba FluoroMax-4). High-resolution TEM images were obtained with a FEI TITAN 80-200 transmission electron microscope. FT-IR spectra were collected by a Thermo Scientific Nicolet 6700 FT-IR. Raman spectra were collected on Horiba Jobin Yvon Lab Ram HR800 Raman system using a 532 nm laser line. AFM images were performed on Bruker Innova atomic force microscope. XPS was obtained on a PHI 5600 X-ray photoelectron spectroscopy and

Auger electron microscopy system. Microscale CD patterns were created using the Sonoplot Microplotter II fluid dispense system.

Femtosecond Transient Absorption Spectroscopy

Our femtosecond transient absorption (fs-TA) setup has been reported before.[63,64] In brief, a 400 nm actinic pump was generated by second harmonic generation (SHG) of fundamental laser pulses (~35 fs duration, 800 nm center wavelength, 1 kHz repetition rate) based on a regenerative amplifier system (Legend Elite-USP-1K-HE Coherent, Inc.). The 400 nm pump was temporally compressed by a prism pair (Suprasil-1, CVI Melles Griot) to ~100 fs duration. The broadband probe, being the supercontinuum white light, was generated by focusing a portion of the fundamental laser output onto a 2-mm-thick quartz cell (Spectrosil 1-Q-2, Starna Cells) filled with deionized water. Depending on the carbon dots (CDs) and peak wavelengths of the relevant excited-state TA features, the probe pulses were compressed by two different sets of chirped mirrors (i.e., DCM-12, 400–700 nm, for green CDs; and DCM-9, 450–950 nm for red CDs) (Laser Quantum, Inc.). The final probe detection windows were set to 415–675 and 500–757 nm for green and red CDs, respectively. During data collection at room temperature (22 °C), the actinic pump power was set at ~0.2 mW before a 500 Hz optical chopper to generate the pump on and off TA spectra for taking the ratio. All CDs were dissolved in dimethylformamide (DMF) solution, and their optical density (OD) at 400 nm was tuned to be ~1 per mm. The CDs sample solution was housed in a 1-mm-thick quartz cell (Spectrosil 1-Q-1, Starna Cells) and constantly stirred by a magnetic staple (i.e., a miniature stir bar) to avoid photodegradation. The actinic pump and probe beams were focused on the sample cell by a parabolic mirror, and only the probe was selected through a pinhole after the sample. The probe that carried the TA signal was collimated and focused into an IsoPlane SCT-320 imaging spectrograph (Princeton Instruments, Inc.), wherein the probe was dispersed by a reflective grating (300 grooves/mm, 300 nm blaze wavelength) and imaged on a CCD array camera (PIXIS:100F, Princeton Instruments, Inc.).[65] The spectral data were calibrated by a HG-1 Mercury Argon calibration light source (Ocean Optics, Inc.) and processed in Igor Pro software (WaveMetrics, Inc.).

Conclusions

In summary, we have successfully demonstrated the synthesis of novel CDs that exhibit red and green emissions with large Stokes shifts of 216 nm and 140 nm, respectively, along with high quantum yields of 45.2% and 24.1%. These remarkable properties make the CDs highly suitable for applications in color-conversion LEDs. The characterization of the R-CDs reveals a multilayer graphene nanodot structure, while the G-CDs, exfoliated from R-CDs, exhibit a monolayer graphene structure. Material and optical analyses indicate that their core and edge states govern the UV excitation of the CDs. The carbonyl groups of the amides on the R-CDs surface and the pyridinic N and hydroxyl groups on the G-CDs surface provide the surface states. These surface states enable electron transition through vibrational relaxation and recombination, leading to light emission at longer wavelengths and contributing to the significant Stokes shift observed in both types of CDs. Fs-TA spectroscopy substantiates this observation, highlighting the two ESA bands' crossover events from edge-to-surface states on the fs to ps timescale, which are more prominent and complete in R-CDs. The pH-dependent emission observed in the CDs provides additional evidence for the significant contribution of surface state-derived emission to the PL mechanism. The edge state-derived excitation allows efficient absorption of near-UV light around 400 nm, making these CDs suitable for color-conversion LED applications. The development of printable CD inks further showcases their versatility, enabling the creation of microscale multicolor fluorescent patterns. These inks were used to demonstrate the fabrication of red and green color-conversion LEDs, highlighting the potential of these CDs in display technologies.

Author Contributions

The manuscript was written through the contributions of all authors. All authors have given approval to the final version of the manuscript.

Conflicts of interest

There are no conflicts to declare.

Acknowledgements

This work was partially supported by National Science Foundation (NSF) grants ECCS-1810067, DMR-1808258, and NNCI-2025489 to L.-J. C., and CHE-2003550 to C.F.

References

1 Y. Liu, H. Huang, W. Cao, B. Mao, Y. Liu and Z. Kang, *Mater. Chem. Front.*, 2020, **4**, 1586–1613.
2 C. Xia, S. Zhu, T. Feng, M. Yang and B. Yang, *Adv. Sci.*, 2019, **6**, 1901316.
3 P. Siahcheshm and P. Heiden, *J. Photochem. Photobiol. A: Chem.*, 2023, **435**, 114284.
4 V. W. Lee, N. Twu and I. Kymissis, *Inf. Disp.*, 2016, **32**, 16–23.
5 Z. Liu, C.-H. Lin, B.-R. Hyun, C.-W. Sher, Z. Lv, B. Luo, F. Jiang, T. Wu, C.-H. Ho, H.-C. Kuo and J.-H. He, *Light Sci. Appl.*, 2020, **9**, 83.
6 J. R. Bonar, G. J. Valentine, Z. Gong, J. Small and S. Gorton, in *Light-Emitting Diodes: Materials, Devices, and Applications for Solid State Lighting XX*, SPIE, 2016, vol. 9768, pp. 92–100.
7 J. Day, J. Li, D. Y. C. Lie, C. Bradford, J. Y. Lin and H. X. Jiang, *Appl. Phys. Lett.*, 2011, **99**, 031116.
8 W.-C. Miao, F.-H. Hsiao, Y. Sheng, T.-Y. Lee, Y.-H. Hong, C.-W. Tsai, H.-L. Chen, Z. Liu, C.-L. Lin, R.-J. Chung, Z.-T. Ye, R.-H. Horng, S.-C. Chen, H.-C. Kuo and J.-H. He, *Adv. Opt. Mater.*, 2023, 2300112.
9 H.-V. Han, H.-Y. Lin, C.-C. Lin, W.-C. Chong, J.-R. Li, K.-J. Chen, P.

Yu, T.-M. Chen, H.-M. Chen, K.-M. Lau and H.-C. Kuo, *Opt. Express,* 2015, **23**, 32504–32515.
10 B.-R. Hyun, C.-W. Sher, Y.-W. Chang, Y. Lin, Z. Liu and H.-C. Kuo, *J. Phys. Chem. Lett.*, 2021, **12**, 6946–6954.
11 H. Zhao, G. Liu, S. You, F. V. A. Camargo, M. Zavelani-Rossi, X. Wang, C. Sun, B. Liu, Y. Zhang, G. Han, A. Vomiero and X. Gong, *Energy Environ. Sci.*, 2021, **14**, 396–406.
12 X. Wang, Y. Zhang, J. Li, G. Liu, M. Gao, S. Ren, B. Liu, L. Zhang, G. Han, J. Yu, H. Zhao and F. Rosei, *Small Methods*, 2022, **6**, 2101470.
13 L. Pan, S. Sun, L. Zhang, K. Jiang and H. Lin, *Nanoscale*, 2016, **8**, 17350–17356.
14 Y. Xian and K. Li, *Adv. Mater.*, 2022, **34**, 2201031.
15 T. Yoshinaga, M. Shinoda, Y. Iso, T. Isobe, A. Ogura and K. Takao, *ACS Omega*, 2021, **6**, 1741–1750.
16 Z.-H. Wen and X.-B. Yin, *RSC Adv.*, 2016, **6**, 27829–27835.
17 Y. Xiao, W. Dong, H. Wang, Y. Hao, Z. Wang, S. Shuang, C. Dong and X. Gong, *Spectrochim. Acta A: Mol. Biomol. Spectrosc.*, 2021, **261**, 120028.
18 J. Hu, Y. Guo, X. Geng, J. Wang, S. Li, Y. Sun, L. Qu and Z. Li, *Chem. Eng. J.*, 2022, **446**, 136928.
19 M. Ali, A. S. Anjum, R. Riaz, A. Bibi, K. C. Sun and S. H. Jeong, *Carbon*, 2021, **181**, 155–168.
20 C. J. Reckmeier, Y. Wang, R. Zboril and A. L. Rogach, *J. Phys. Chem. C*, 2016, **120**, 10591–10604.
21 Y. Chen, H. Lian, Y. Wei, X. He, Y. Chen, B. Wang, Q. Zeng and J. Lin, *Nanoscale*, 2018, **10**, 6734–6743.
22 V. Gude, A. Das, T. Chatterjee and P. K. Mandal, *Phys. Chem. Chem. Phys.*, 2016, **18**, 28274–28280.
23 S. Zhang, H. Wang, Y. Li, F. Y. Data, Q. Wang and L. Jiao, *Mater. Lett.*, 2020, **263**, 127208.
24 Q. Liu, X. Niu, K. Xie, Y. Yan, B. Ren, R. Liu, Y. Li and L. Li, *ACS Appl. Nano Mater.*, 2021, **4**, 190–197.
25 F. Yan, Z. Bai, F. Zu, Y. Zhang, X. Sun, T. Ma and L. Chen, *Microchim Acta*, 2019, **186**, 113.
26 S. Zhang, X. Ji, J. Liu, Q. Wang and L. Jin, *Spectrochim. Acta A: Mol. Biomol. Spectrosc.*, 2020, **227**, 117677.
27 J. Li, H. Zhao, X. Zhao and X. Gong, *Nanoscale Horiz.*, 2023, **8**, 83–94.
28 T. Zhang, J. Zhu, Y. Zhai, H. Wang, X. Bai, B. Dong, H. Wang and H. Song, *Nanoscale*, 2017, **9**, 13042–13051.
29 H. Ding, J.-S. Wei, P. Zhang, Z.-Y. Zhou, Q.-Y. Gao and H.-M. Xiong, *Small*, 2018, **14**, 1800612.
30 X. Miao, D. Qu, D. Yang, B. Nie, Y. Zhao, H. Fan and Z. Sun, *Adv. Mater.*, 2018, **30**, 1704740.
31 X. T. Zheng, A. Ananthanarayanan, K. Q. Luo and P. Chen, *Small*, 2015, **11**, 1620–1636.
32 A. Cuesta, P. Dhamelincourt, J. Laureyns, A. Martínez-Alonso and J. M. D. Tascón, *Carbon*, 1994, **32**, 1523–1532.
33 M. J. Matthews, M. A. Pimenta, G. Dresselhaus, M. S. Dresselhaus and M. Endo, *Phys. Rev. B*, 1999, **59**, R6585–R6588.
34 L. Cao, M. Zan, F. Chen, X. Kou, Y. Liu, P. Wang, Q. Mei, Z. Hou, W.-F. Dong and L. Li, *Carbon*, 2022, **194**, 42–51.
35 D. Geng, S. Yang, Y. Zhang, J. Yang, J. Liu, R. Li, T.-K. Sham, X. Sun, S. Ye and S. Knights, *Appl. Surf. Sci.*, 2011, **257**, 9193–9198.
36 M. Kim, S. Hwang and J.-S. Yu, *J. Mater. Chem.*, 2007, **17**, 1656-1659.
37 V. Ţucureanu, A. Matei and A. M. Avram, *Crit. Rev. Anal. Chem.*, 2016, **46**, 502–520.
38 D. Qu, M. Zheng, P. Du, Y. Zhou, L. Zhang, D. Li, T. Huaqiao, Z. Zhao, Z. Xie and Z. Sun, *Nanoscale*, 2013, **5**, 12272-12277.
39 R. M. Yadav, Z. Li, T. Zhang, O. Sahin, S. Roy, G. Gao, H. Guo, R. Vajtai, L. Wang, P. M. Ajayan and J. Wu, *Adv. Mater.*, 2022, **34**, 2105690.
40 H. Nie, M. Li, Q. Li, S. Liang, Y. Tan, L. Sheng, W. Shi and S. X.-A. Zhang, *Chem. Mater.*, 2014, **26**, 3104–3112.
41 Y. Zhang, R. Yuan, M. He, G. Hu, J. Jiang, T. Xu, L. Zhou, W. Chen, X. Weidong and X. Liang, *Nanoscale*, 2017, **9**, 17849-17858.
42 M. J. McAllister, J.-L. Li, D. H. Adamson, H. C. Schniepp, A. A. Abdala, J. Liu, M. Herrera-Alonso, D. L. Milius, R. Car, R. K. Prud'homme and I. A. Aksay, *Chem. Mater.*, 2007, **19**, 4396–4404.
43 W. W. Liu and J. N. Wang, *Chem. Commun.*, 2011, **47**, 6888.
44 B. Zhang, G. An, J. Chen, H. Guo and L. Wang, *J. Colloid Interface Sci.*, 2023, **637**, 173–181.
45 Z. Wang, G. Li, W. Hou, H. Guo, L. Wang and M. Wu, *ACS Nano*, 2023, **17**, 8671–8679.
46 Z.-H. Sheng, L. Shao, J.-J. Chen, W.-J. Bao, F.-B. Wang and X.-H. Xia, *ACS Nano*, 2011, **5**, 4350–4358.
47 H. Wang, P. Haydel, N. Sui, L. Wang, Y. Liang and W. W. Yu, *Nano Res.*, 2020, **13**, 2492–2499.
48 L. Zhao, F. Di, D. Wang, L.-H. Guo, Y. Yang, B. Wan and H. Zhang, *Nanoscale*, 2013, **5**, 2655.
49 M. Liu, *NAT*, 2020, **1**, 1–12.
50 C. Chen, Z. Xu, J. Qiu, W. Ye, X. Xu, R. Wang, C. Hu, J. Zhuang, B. Lei, W. Li, X. Zhang, G. Hu and Y. Liu, *ACS Appl. Nano Mater.*, 2022, **5**, 9140–9149.
51 Y. Dong, H. Pang, H. B. Yang, C. Guo, J. Shao, Y. Chi, C. M. Li and T. Yu, *Angew. Chem. Int. Ed.*, 2013, **52**, 7800–7804.
52 J. Zhu, X. Bai, J. Bai, G. Pan, Y. Zhu, Y. Zhai, H. Shao, X. Chen, B. Dong, H. Zhang and H. Song, *Nanotechnology*, 2018, **29**, 085705.
53 D. Chen, W. Wu, Y. Yuan, Y. Zhou, Z. Wan and P. Huang, *J. Mater. Chem. C*, 2016, **4**, 9027–9035.
54 D. Chen, H. Gao, X. Chen, G. Fang, S. Yuan and Y. Yuan, *ACS Photonics*, 2017, **4**, 2352–2358.
55 Q. An, Q. Lin, X. Huang, R. Zhou, X. Guo, W. Xu, S. Wang, D. Xu and H.-T. Chang, *Dyes Pigm.*, 2021, **185**, 108878.
56 P. Lazar, R. Mach and M. Otyepka, *J. Phys. Chem. C*, 2019, **123**, 10695–10702.
57 K. R. Geethalakshmi, T. Y. Ng and R. Crespo-Otero, *J. Mater. Chem. C*, 2016, **4**, 8429–8438.
58 S. H. Jin, D. H. Kim, G. H. Jun, S. H. Hong and S. Jeon, *ACS Nano*, 2013, **7**, 1239–1245.
59 M. A. Eriksson, T. Härd and L. Nilsson, *Biophys. J.*, 1995, **69**, 329–339.
60 H. A. Nguyen, I. Srivastava, D. Pan and M. Gruebele, *Proc. Natl. Acad. Sci. U.S.A.*, 2021, **118**, e2023083118.
61 X. Wen, P. Yu, Y.-R. Toh, X. Hao and J. Tang, *Adv. Opt. Mater.*, 2013, **1**, 173–178.
62 L. Sui, W. Jin, S. Li, D. Liu, Y. Jiang, A. Chen, H. Liu, Y. Shi, D. Ding and M. Jin, *Phys. Chem. Chem. Phys.*, 2016, **18**, 3838–3845.
63 W. Liu, Y. Wang, L. Tang, B. G. Oscar, L. Zhu and C. Fang, *Chem. Sci.*, 2016, **7**, 5484–5494.
64 L. Tang, L. Zhu, M. Taylor, Y. Wang, S. Remington and C. Fang, *Molecules*, 2018, **23**, 2226.
65 C. Fang, L. Tang, B. G. Oscar and C. Chen, *J. Phys. Chem. Lett.*, 2018, **9**, 3253–3263.